<Review article>

Glymphatic Imaging using MRI

Toshiaki Taoka M.D., Ph. D. and Shinji Naganawa M.D., Ph. D.

Department of Radiology, Nagoya University

Corresponding author:
Toshiaki Taoka M.D., Ph. D.
Department of Radiology, Nagoya University,
65 Tsurumai-cho, Showa-ku, Nagoya,
Aichi, 466-8550 Japan
Tel: +81-52-744-2328
Fax: +81-52-744-2335
e-mail: ttaoka@med.nagoya-u.ac.jp

Running Title：Glymphatic Imaging

Abstract

In recent years, the existence of a mass transport system in the brain via cerebrospinal fluid (CSF) or interstitial fluid (ISF) has been suggested by many studies. The glymphatic system is hypothesized to be a waste clearance system of the CSF through the perivascular and interstitial spaces in the brain. Tracer studies have primarily been used to visualize or evaluate the waste clearance system in the brain, and evidence for this system has accumulated. The initial study that identified the glymphatic system was an in vivo tracer study in mice. In that study, fluorescent tracers were injected into the cisterna magna and visualized by two-photon microscopy. MRI has also been used to evaluate glymphatic function primarily with gadolinium-based contrast agents (GBCAs) as tracers. A number of GBCA studies evaluating glymphatic function have been conducted using either intrathecal or intravenous injections. Stable isotopes, such as ^{17}O-labeled water, may also be used as tracers since they can be detected by MRI. In addition to tracer studies, several other approaches have been used to evaluate ISF dynamics within the brain, including diffusion imaging. Phase contrast evaluation is a powerful method for visualizing flow within the CSF space. In order to evaluate the movement of water within tissue, diffusion-weighted MRI represents another promising technique, and several studies have utilized diffusion techniques for the evaluation of the glymphatic system. This review will discuss the findings of these diffusion studies.

Key words: glymphatic system, cerebrospinal fluid, interstitial fluid, magnetic resonance imaging, diffusion imaging, contrast media

“Neurofluids” and common spaces within the brain

Mass transport within brain tissue is primarily mediated by fluid flow. Needless to say, blood plays the most prominent role in this mass transport. The requirements for metabolism in the brain, including oxygen and glucose, are carried to the brain by blood flow and delivered to the brain through the blood brain barrier. However, blood is not the sole mediator of mass transport in the brain. Recently, mass transport through the cerebrospinal fluid (CSF) or interstitial fluid (ISF) has been gaining attention as an important factor in brain homeostasis. While tissues outside of the brain have lymphatic systems for clearance of metabolic waste, it was previously thought that the brain lacked such a system. Based on their experiments, Iliff and Nedergaard et al. first hypothesized that the brain also possesses its own waste clearance system and termed it the “glymphatic system”, which was coined by combining “G” for glia with “lymphatic” system (1,2). In their hypothesis, the perivascular spaces within the brain function as a conduit for CSF flow into the brain parenchyma. The perivascular space around the arteries allows CSF to enter the interstitial spaces through water channels controlled by aquaporin 4 (AQP4). CSF entering the interstitial space washes away waste proteins within the tissue. The CSF or ISF that gets flushed out between cells flows into the perivascular space around veins and is discharged outside of the brain (Figure 1a). Recently, Iliff et al. provided a comprehensive definition of this system as “a brain-wide perivascular network that supports the exchange of ISF and CSF, facilitating the clearance of interstitial solutes, including amyloid β and tau from the brain parenchyma” (3). Under this glymphatic system hypothesis, the interstitial space in the brain is regarded as common space, which not only acts as a supportive structure, but also functions as a space for mass transport, immune function and intercellular signal transmission. Following the introduction of the glymphatic system hypothesis, an increasing number of studies have been published which attempted to describe fluid dynamics within the brain. Accordingly, in 2018 and 2019, the annual meeting of the International Society for Magnetic Resonance in Medicine (ISMRM) held sessions to discuss the topic of “neurofluids”. The word “neurofluids” was first proposed by Prof. E. F. Toro from the University of Trento as the name for a project to explore the fluid dynamics within the central nervous system (CNS), and this word has been used to indicate all types of fluids within the CNS, including CSF, ISF, and blood. Although this term has not been formally defined or authenticated, it seems an apt description for the inclusive evaluation of fluid dynamics within the CNS(Figure 1b). Many published reports have attempted to visualize or define the fluid dynamics within the CNS, including the glymphatic hypothesis, using tracer studies or other methods. In the present review, we will discuss these attempts and the results from imaging the glymphatic system by MRI.

Methods for visualizing the glymphatic system and neurofluid dynamics

Tracer studies

In order to visualize or evaluate mass transport systems in the living body, tracer studies are one of the most efficient methods. Tracer studies allow the analysis of a substance and its interactions in the body by labeling the substance in a manner that does not alter its original properties (4). In the brain, tracer studies have been used to simulate or trace transport within the interstitial space (5). In addition to small radioactive particles, tracers can have other characteristics that can be quantitatively assessed as well as physical characteristics that can be detected after extended periods of time, such as temperature. Radio isotopes (RI) are generally used tracers for imaging in the medical field. RI cisternography by ^{111}In-DTPA has long been used for the evaluation of CSF dynamics. CT cisternography using an iodine contrast agent has also been utilized for the evaluation of hydrocephalus or other CSF abnormalities. However, there have been no reports evaluating the glymphatic system by RI cisternography or CT cisternography, mainly because these tracer studies require ionized radiation.

Laser microscopy tracer studies using fluorescent agents

The original studies supporting the glymphatic system hypothesis involved observations of the subcortical region (at a depth of 100 μm) of the mouse brain *in vivo* by two-photon imaging using a fluorescent tracer and laser-scanning microscope. This technique is capable of visualizing the living brain through the dura using highly permeable infrared laser light. Two-photon laser-scanning microscopy is invasive in that it requires the removal of a portion of the animal's cranial bone, and visualization is limited to the subcortical regions. However, this method enables real-time in vivo observations and can examine differences in behavior based on molecular size. In these experiments, while large molecular weight fluorescent tracers entered the brain along the perivascular spaces, they did not enter the surrounding interstitial space. This is in contrast to small molecular weight fluorescent tracers that were concentrated in the perivascular spaces and entered the interstitium from both the paravascular space and from the pial surface (1).

With these types of fluorescent tracer studies, important findings on the relationship between the glymphatic system and sleep have been uncovered. Xie et al. infused fluorescent tracers into the subarachnoid CSF via a cannula implanted in the cisterna magna for real-time assessment of tracer movement in the CSF by in vivo two-photon imaging comparing CSF influx into the cortex

of awake, anesthetized, and sleeping mice. They found that natural sleep or anesthesia were associated with a 60% increase in the interstitial space, resulting in a striking increase in convective exchange of CSF with ISF (6).

MRI tracer studies using intrathecal injection of gadolinium-based contrast agent

After the initial publication by Iliff et al., follow-up experiments investigated the glymphatic system hypothesis in MRI studies using intrathecal administration of gadolinium-based contrast agent (GBCA) as a tracer (7,8). In contrast to observations of a fluorescent tracer by laser-scanning microscopy which can only visualize the surface of the brain, MRI is a method that provides tomographic images and evaluation of the whole brain. Iliff et al. reported on the use of MRI to visualize glymphatic function in the rat brain in vivo by dynamic contrast-enhanced MRI following intrathecal contrast agent administration. This approach is capable of characterizing both the kinetics and spatial distribution of glymphatic function throughout the entire brain. They compared the influx of small molecular weight Gd-DTPA with large molecular weight polymeric Gd-chelate over the early infusion period, and the dynamic time series of MR images that captured the transport of Gd-DTPA and large molecular weight polymeric Gd-chelate through the glymphatic system demonstrated clear differences in whole-brain distributions between the small and large molecules (7). Gaberel et al. conducted in vivo animal experiments to measure the influence of stroke on perfusion in the glymphatic system using MRI after intrathecal injection of a gadolinium chelate within the cisterna magna. The mouse models of stroke included subarachnoid hemorrhage (SAH), intracerebral hemorrhage, carotid ligature, and embolic ischemic stroke; they showed that the glymphatic system was severely impaired after SAH and in the acute phase of ischemic stroke, but was not altered after carotid ligature or intracerebral hemorrhage. In addition, they found that glymphatic perfusion after SAH can be improved by intracerebroventricular injection of tissue-type plasminogen activator (8).

In humans, several studies have been reported in which intrathecally administrated GBCA was used as a tracer for clinical diagnosis or evaluation of glymphatic function (9). As might be expected, the use of intrathecal administration of GBCA has yet to be approved in any country (10). Intrathecal administration of high-dose GBCA may cause serious gadolinium encephalopathy which can cause symptoms including nausea, dyspnea, subjective chills, delirious state with somnolence, dysarthria, spastic pain of the lower extremities, limb ataxia and gaze evoked nystagmus, and a case of fatality has even been reported (11-14). However, there are several institutions in which intrathecal administration of GBCA can be performed in human subjects for the purpose of clinical diagnosis with thoughtful consideration as to appropriate

dosing and approval from their institutional review board (15,16). The intrathecal administration of GBCA has been reported for use in diagnosing idiopathic normal pressure hydrocephalus (iNPH), aqueductal stenosis, evaluating third ventriculostomy, or detecting CSF leakage including cases with difficult leakage from the skull base (17-19). Several studies using intrathecal administration of GBCA focused on the evaluation of glymphatic function in the brain. Eide et al. reported a case that underwent MRI with intrathecal administration of gadobutrol, which was found to be distributed throughout the brain after 1 and 4.5 h (15). The same group conducted a clinical study using this methodology for cases of iNPH. Ringstad et al. attempted to image CSF/ISF dynamics and glymphatic function in humans, and conducted MRI studies with intrathecal GBCA as a CSF/ISF tracer in a prospective study of iNPH patients and control subjects. After intrathecal administration of GBCA, they observed enhancement in the brain parenchyma, subarachnoid and intraventricular spaces, and within the sagittal sinus at every imaging time point. In all study subjects, GBCA was propagated anterogradely along the large leptomeningeal arteries at the brain surface. They found a flow pattern characteristic of iNPH in which ventricular reflux of GBCA from the subarachnoid space was followed by transependymal GBCA migration, and delayed enhancement and decreased clearance of GBCA at the Sylvian fissure. They also found that parenchymal enhancement peaked overnight in both iNPH patients and control subjects, although the peak was larger in iNPH patients; these results may indicate a crucial role for sleep. They interpreted the decreased GBCA clearance from the subarachnoid space, along with the persistent enhancement in the brain parenchyma, as signs of reduced glymphatic clearance in iNPH patients (Figure 2) (20).

MRI tracer studies using intravenous injection of gadolinium-based contrast agent

Only a limited number of experimental animal studies have attempted to evaluate glymphatic function by intravenous administration of GBCA. This may be due to the relatively easy ability to directly deliver GBCA as a tracer for CSF dynamics by intrathecal injection. Taoka et al. conducted MRI experiments using intravenous GBCA administration in rats to evaluate the short-term dynamics of signal intensity changes in the brain parenchyma and CSF space. After intravenous injection of high-dose GBCA (1 mmol/kg), the fourth ventricle showed an instantaneous increase in signal intensity (21). The signal curve of the cerebral cortex and deep cerebellar nuclei reached peak signal intensity later than the fourth ventricle, but earlier than the prepontine cistern. This time course suggests that the gadodiamide distribution in the cerebral cortex and deep cerebellar nuclei are dependent on both blood flow and CSF. These findings confirmed the results from previous studies that had suggested that CSF is one potential route for

entry of gadolinium-based contrast agent into the brain (15,16). Another intravenous GBCA injection experiment was conducted to evaluate the concentration of retained gadolinium within the rat brain after repeated intravenous administration of gadodiamide at different times of the day and with varying levels of anesthesia. Rats were divided into 4 groups according to injection time (morning or late afternoon) and anesthesia duration (none, short, and long) during administration. All animals received a high dose of GBCA (gadodiamide 1.8 mmol/kg, 8 times over 2 weeks); 5 weeks after the last administration, gadolinium concentration in dissected brain tissues was quantified by inductively coupled plasma mass spectrometry. Results showed that the concentration of gadolinium in the brains of the morning injection group was significantly lower than that in the late afternoon injection group. The lowest concentration of gadolinium was found in the group injected in the morning under long anesthesia (21). The results could be explained by a higher glymphatic clearance after the morning injection, and reduced glymphatic activity after injection in the late afternoon. Because rats are nocturnal animals, the glymphatic system is expected to be more active during the day (6). Moreover, anesthesia seemed to facilitate the glymphatic clearance of gadodiamide, especially when administered for longer durations (21).

Similarly, in human studies with intravenous administration of GBCA, transition into the brain parenchyma has been reported. One study sought to evaluate the degree of blood-brain barrier (BBB) leakage using the Patlak graphical approach which was found to be the most appropriate model for low-leakage conditions. The study enrolled patients with early Alzheimer's disease (AD) and healthy age-matched control subjects, and subjects underwent dynamic GBCA enhanced MRI for 25 minutes; subsequent histogram analysis was used to determine the volume fraction of the leaky brain tissue. Results showed that the BBB leakage rate was significantly higher in the total gray matter and cortex in AD patients compared with control subjects, suggesting that a compromised BBB may contribute to the cascade of pathologic events that eventually leads to cognitive decline and dementia (22). Several other studies have evaluated the extended longitudinal behavior of intravenously administrated GBCA as a tracer in a series of experiments utilizing heavily T2-weighted 3D-FLAIR (hT2-FL) images to visualize the small amount of GBCA in the CSF space (23-26). Naganawa et al. reported enhancement in the perivascular space (PVS) 4 h after intravenously administrated GBCA, even in subjects without renal insufficiency (23). It is interesting that this PVS enhancement was not seen in the giant perivascular space, which may suggest that the giant perivascular space is isolated from other CSF spaces (24). Furthermore, they reported signal intensity differences between the perivascular space in the basal ganglia and white matter on pre-contrast images, which seemed to suggest that the fluid composition might be different between these perivascular spaces. To further evaluate

this contrast enhancement effect, significant enhancement was observed in the perivascular space in the basal ganglia, the CSF in the ambient cistern, and the CSF in the Sylvian fissure compared to the pre-contrast scan, while no significant contrast enhancement was observed in the perivascular space in the white matter. This difference in contrast enhancement may suggest a difference in the drainage function of these regions (25). The leakage of GBCA into the CSF space was particularly evident in regions surrounding large cortical veins such as the vein of Labbe. Very interestingly, GBCA leakage from the cortical veins was seen in older subjects (greater than 37 years old), but not in younger subjects (less than 37 years old), and the area exhibiting GBCA leakage around the cortical veins showed a significant correlation only with age (Figure 3) (26). These results suggest that chronic hypoxic and/or inflammatory processes in the cortex and leptomeninges during the aging process may underlie these observations.

A tracer study using GBCA has also been reported for the visualization of the meningeal lymphatic vessels (27). Meningeal lymphatic vessels were recently discovered to be lining the dural sinuses. These structures express the molecular hallmarks of lymphatic endothelial cells, are able to carry both fluid and immune cells from the cerebrospinal fluid, and are connected to the deep cervical lymph nodes (28). On T2-FLAIR and T1-weighted black-blood imaging in human subjects, lymphatic vessel enhancement was visualized using a standard GBCA, and localized around the dural sinuses, middle meningeal artery, and cribriform plate, but could not be observed with a blood-pool type GBCA(27).

MRI tracer studies using gadolinium-based contrast agent and gadolinium deposition in the brain

Results from intrathecal GBCA administration studies likely provide important information when considering the cause of gadolinium (Gd) deposition in the brain. Gd deposition in the brain after repeated administration of GBCA was reported by Kanda et. al in 2014 (29-31). They showed a signal increase in the dentate nucleus and globus pallidus on plain T1-weighted images which correlated with the frequency of GBCA administration, and showed the potential for Gd deposition within tissues. This phenomenon following repeat administration of GBCA was confirmed in many clinical practices as well as by histological studies. Oner et al. conducted a systematic study of intrathecal administration of GBCA (16). This comparative evaluation of MRI before and after intrathecal administration was conducted in patients with normal renal function and a history of intrathecal administration of linear GBCA but that had never experienced an intravenous injection of GBCA. Visual assessments and quantitative evaluations were carried out in the globus pallidus, putamen, and dentate nuclei for all subjects. Quantitative evaluation

confirmed a signal increase in all cases compared with pre-intrathecal administration. These findings suggest that Gd deposition in the basal ganglia might occur through a pathway from the CSF. Furthermore, the results also suggest that the glymphatic system may, at least in part, be involved in the Gd distribution pathway into brain tissue. Combined with the findings that GBCA gets distributed within the CSF cavity and perivascular spaces within several hours after administration of contrast medium (Figure 4) (23), we proposed a hypothesis for the behavior of Gd after intravenous injection (32). Most intravenously administered GBCA is excreted via the kidneys by systemic circulation, and the concentration of GBCA in the cerebral blood vessels also decreases rapidly. However, some GBCA is distributed to the CSF and ISF, so is taken into glymphatic circulation. Although the concentration of GBCA in the glymphatic system is low, it takes considerable time for it to wash out; therefore, the brain tissue will be exposed to GBCA-containing CSF over a longer period of time. At the same time, as de-chelation of linear GBCA occurs via an unknown mechanism, deposition of Gd in the brain tissue may also occur (Figure 5) (32).

MRI tracer studies using stable isotopes

While there are three stable isotopes of oxygen (^{16}O,^{17}O and ^{18}O), only ^{17}O can produce a signal by MRI since it has an odd number of electrons. The methods for visualizing ^{17}O as a tracer include direct and indirect techniques. Due to the low gyromagnetic ratios of ^{17}O, the direct method suffers from a poor signal-to-noise ratio and lower spatial resolution (33). In addition, the direct method requires specific hardware for ^{17}O detection (34). The indirect method is based on proton T1ρ-dispersion and methods utilizing T2 shortening of ^{17}O-induced proton signals based on scalar coupling between ^{17}O and ^{1}H (33-35). One animal study has used the indirect method for evaluating CSF dynamics. In these experiments, ^{17}O-labeled water ($H_2{}^{17}O$) was intravenously administrated in vivo to AQP-1 (expressed in the choroid plexus epithelium) and AQP-4 (expressed in the perivascular end-feet of astrocytes) knockout mice, and water influx to the brain was indirectly observed using T2-weighted images. Results showed that the behavior of water molecules in AQP-1 knockout mice was virtually identical to that of wild type mice. In contrast, the penetration and steady concentration of $H_2{}^{17}O$ in the third ventricle was significantly reduced in AQP-4 knockout mice. These observations seem to indicate that water influx into the CSF is regulated by AQP-4, known to be responsible for water homeostasis of the perivascular space, and not by AQP-1 which is found in the choroid plexus. Thus, water movement within the perivascular space is critical for CSF volume homeostasis (35).

The analysis of $H_2{}^{17}O$ has also been reported in humans. Kudo et al. utilized dynamic

steady-state sequences to detect the T2-shortening effect by $H_2{}^{17}O$ (34). After intravenous injection of $H_2{}^{17}O$, signal changes relative to the baseline were calculated, and kinetic analyses of the time-to-signal change curves were conducted. Their results showed different kinetic parameters between the brain parenchyma and CSF spaces. The cerebral cortex and subarachnoid spaces on the brain surface showed a prompt signal drop indicating quick transmission of $H_2{}^{17}O$ to these regions, and suggestive of fluid leakage from vessels or the surface of the brain. In contrast, the signal drop in the ventricle containing the choroid plexus was significantly delayed, indicating that fluid exchange is less active in the ventricle (Figure 6) (34).

MRI tracer studies using an inversion pulse

Tracer studies have not been limited to the use of particles or other substances such as isotopes. In the field of magnetic resonance, magnetization can also be used as a tracer. Spatial modulation of magnetization (SPAMM) is one of the motion-sensitive MR techniques for visualizing the motion of the brain parenchyma or CSF through non-selective radiofrequency pulses separated by gradient pulses to create a series of stripes across the image produced by saturated magnetization (36). Several studies have been published using this technique to evaluate CSF motion for the assessment of hydrocephalus or other abnormalities in CSF dynamics (36,37). For example, the SPAMM technique was used to demonstrate that CSF pulsatile motion is restored after craniovertebral junction decompression surgery in cases of Chiari malformation (37).

Time-spatial labeling inversion pulse (Time-SLIP) MRI is another approach for the visualization of CSF motion by applying a slab of inversion pulse at the region of interest in the CSF space, which utilizes CSF as a tracer by magnetization. This method allows CSF dynamics to be depicted under physiological conditions since it does not require an extrinsic tracer. Findings obtained with the Time-SLIP method contrasted with the conventional ideas of CSF physiology. One of the findings was that CSF flow occurs from the third ventricle to the lateral ventricles in healthy persons, suggesting that CSF is actively exchanged between the lateral ventricles and the third ventricle through the foramen of Monro in the normal brain. In contrast, no CSF reflux from the third ventricle to the lateral ventricles was observed in patients with hydrocephalus (38,39).
MRI tracer studies using an inversion pulse to the arterial blood, that is, the arterial spin labelling method, have also been attempted for the evaluation of glymphatic function. In an animal study, multiple echo time arterial spin labelling was applied to the mouse brain to assess blood-brain interface (BBI) water permeability by calculating the exchange time of magnetically labelled

intravascular water across the BBI. Results showed a 31% increase in the exchange time in AQP4-deficient mice compared to their wild-type counterparts, demonstrating the sensitivity of the multiple echo time arterial spin labelling technique to the absence of AQP4 water channels (40).

Other methods using MRI

Phase contrast methods

In magnetic resonance, a phase shift of the spin occurs when the spin moves along a magnetic gradient, and the degree of phase shift depends on the velocity of the spin. The phase contrast method has been utilized to visualize fluid flow in the body, including arterial or venous blood, and the velocity of the CSF can also be measured by this method. Recently, the visualization of CSF dynamics by four-dimensional phase-contrast (4D-PC), which can acquire three spatial dimensions and one dimension hemodynamic data, has been used to depict fluid dynamics including velocity vectors and 3D streamlines. One of the advantages of 4D-PC is that this method can directly and noninvasively measure human intracranial arterial hemodynamics in individual subjects (41). The 4D-PC method has also been used to quantify the spatiotemporal velocity distribution of CSF motion as vector cine images (42). The 4D-PC technique can visualize the propagation of pulsatile CSF motion even in spaces separated by a thin membrane-like structure through which no spin travels, such as the Liliequist membrane or an arachnoid cyst wall (43). One report questioned the traditional theory that the driving force of CSF flow is choroid plexus pulsation. In that report, the median CSF velocity was significantly lower in the posterior part of the lateral ventricle than in other regions on 4D-PC, and Time-SLIP images showed suppressed CSF motion around the choroid plexus in the trigone (44). Based on their results of CSF velocity using the 4D-PC method, they suggested that the driving force of CSF might be the squeezing pump action of the thalamus on the ventricular system. In addition, blood pulsation of the vascular system was also speculated to be directly propagated to the CSF. Another study using 4D-PC reported a decrease in CSF flow velocity by as much as 30% with the compression of the bilateral jugular veins (45). While these studies demonstrate that phase contrast methods are powerful tools for evaluating CSF dynamics within ventricles or the subarachnoid space, it has generally been difficult to evaluate the movement or dynamics of ISF within brain parenchyma using phase contrast methods. However, one study attempted to evaluate creeping flows by phase contrast MRI using stimulated echo (46). Although the report was just a theoretical consideration involving a phantom study, and verification in animals or humans was not presented, the method has the potential to be a tool for evaluating ISF dynamics in the brain parenchyma.

Diffusion imaging

Evaluation of diffusion phenomena using magnetic resonance techniques was first reported by Stajskal and Tanner (47); LeBihan et al. then applied this diffusion technique for the first time in MR imaging (48). In the diffusion image technique, a pair of motion providing gradients (MPG), which are magnetic field gradients for detecting self-diffusion of water molecules, are added with an inverted pulse of 180 degrees between them. While the phase change of the stationary molecule is canceled to maintain the signal, the phase change of the moving molecule is not canceled but is expressed as a decrease in signal based on the amount of movement. The generally used index for the strength of the MPG is the b value, which is given by $b=\gamma^2G^2\delta^2(\Delta-\delta/3)$, where γ: gyromagnetic ratio, G: strength of the MPG, Δ: interval of the MPG and δ: duration of the MPG. On diffusion weighted images, tissues with strong diffusion are depicted as low signal and tissues with limited diffusion are depicted as high signal. In the Stajskal and Tanner method, the diffusion coefficient can be calculated by obtaining the slope of the graph from the logarithmic values of the signal of different b-values. In neuronal tissues, diffusion of water molecules is not uniform in all directions. Due to the structure of the cell membranes or other structures within the tissue the speed of diffusion varies depending on the direction, resulting in a state called anisotropic diffusion. In the white matter of the brain, diffusion perpendicular to the direction of the nerve fibers is more limited than in the same direction of the nerve fibers. The diffusivity differs depending on the direction of the motion probing gradient. Scalars and vectors are not sufficient to analyze this status, and the concept of a tensor is needed. A tensor is a multidimensional array. When expressing diffusion in a three-dimensional space, a 3×3 matrix form is used, and diffusion tensor imaging (DTI) is the method designed to obtain it.

Diffusion MRI methods are also used to evaluate the dynamics of CSF or ISF. While phase contrast methods cannot evaluate the motion of ISF in the brain parenchyma, diffusion methods are able to evaluate water molecule dynamics in brain tissue by signal changes in motion-probing gradients. When compared to tracer studies, diffusion-based techniques provide very different information. Tracer studies evaluate the behavior of a tracer through time, in other words, information by integration. Tracer studies of the glymphatic system require hours to follow the distribution of the tracer within the brain, and thus monitoring the activity of the glymphatic system in real-time is not possible. In contrast, diffusion methods provide information on water molecules in tissues at the moment motion-probing gradients are applied, that is information by differentiation. Diffusion images, including DTI, can be acquired within several minutes, and may also have the potential to monitor glymphatic system status over time. In addition, methods based

on diffusion imaging are non-invasive compared to tracer studies which require intrathecal or intravenous injection of tracers.

There have been several attempts to analyze ISF dynamics in the brain and to evaluate the function of the glymphatic system using diffusion-based techniques. One technique is called "diffusion tensor image analysis along the perivascular space (DTI-ALPS)" (Figure 7) (49). With this method, the motion of water molecules in the direction of the perivascular space is evaluated by measuring diffusivity using the diffusion tensor method. The medullary arteries and veins are the vessels of the brain parenchyma that accompany the perivascular space, which is the major drainage pathway of the glymphatic system. At the level of the lateral ventricle body, the medullary veins run perpendicular to the ventricular wall (50,51), and the perivascular space is oriented in the same direction as the medullary veins – in a right-left direction (x-axis). In this region, projection fibers run in the head-to-foot (z-axis) direction, mainly adjacent to the lateral ventricle, and superior longitudinal fascicles (SLFs) representing the association fibers run in the anterior-posterior (y-axis) direction outside the projection fibers. Outside of the SLFs, subcortical fibers mainly run in the right-left (y-axis) direction in subcortical regions. Consequently, within this area the perivascular space runs perpendicular to the projection fibers and SLFs. This conformation of the perivascular space and major fibers allows nearly independent analysis of the diffusivity along the direction of the perivascular space because the major fiber tracts are not parallel to the direction of the perivascular space. When common changes in diffusivity in the right-left direction (x-axis) in both the projection fiber area and association fiber area are present, the changes are the result of alterations in the diffusivity in this direction that corresponds with the direction of the perivascular space. In order to evaluate the activity of the glymphatic system in individual subjects, diffusion tensor image analysis along the perivascular space (DTI-ALPS) is calculated as ALPS-scores. This score is determined by the ratio of two sets of diffusivity values which are perpendicular to the dominant fibers in the tissue. In the area of the projection fibers, the dominant fibers run in the direction of the z-axis, and both the x and y axes are perpendicular to the dominant fibers. Similarly, in the area of the association fibers, the dominant fibers run in the direction of the y-axis, and both the x and z axes are perpendicular to the dominant fibers. The major differences in water molecule behavior between x-axis diffusivity in both areas (Dxx*proj* and Dxx*assoc*) and the diffusivity which is perpendicular to them (Dyy*proj* and Dzz*assoc*) is the existence of the perivascular space. It has been hypothesized that the ratio of these should indicate the influence of water diffusion along the perivascular space which reflects the activity of the glymphatic system in individual subjects. If the ratio is close to 1, the influence of water diffusion along the perivascular space is at a minimum, and a larger ratio indicates greater water diffusivity

along the perivascular space. In our results, significant positive correlations were observed between the ALPS-index and Mini-Mental State Examination (MMSE) scores. This suggests that the ALPS-index can be used to evaluate the activity of the glymphatic system in individual cases (49). Another study aimed to replicate the DTI-ALPS method in 36 patients with AD and associated status (16 AD, 16 MCI, and 4 SMC), and showed significant correlations between DTI-ALPS and stratified MMSE scores (52). The DTI-ALPS method has also been used for the evaluation of glymphatic function in iNPH. Cekic et al. reported that the ALPS-index can reliably distinguish between iNPH, ventriculomegaly/pseudo-iNPH, and control groups. In particular, the ALPS-index performed better than both the Evans index (AUC = 1.00 vs. 0.84, p = 0.028) and the callosal angle (AUC = 1.00 vs. 0.74, p = 0.016) in distinguishing between pseudo-iNPH and iNPH (53).

Other methods using diffusion imaging to evaluate glymphatic function have recently been introduced. An animal model was described for evaluating glymphatic function using an ultra-long echo time, low b-value, multi-direction diffusion-weighted MRI sequence to assess perivascular fluid movement. Results of these experiments indicated a 300% increase in fluid movement in the perivascular space as the vessels pulsate with each heartbeat (54). In human subjects, one report utilized DTI to detect changes in glymphatic function based on circadian rhythms, that is fluctuations with time of day. In that report, a conventional mono-exponential tensor model was used to assess daily fluctuations in DTI parameters with a dual compartment tensor model that allowed for direct assessment if changes in DTI measures were due to an increase in the CSF/free-water volume fraction or due to an increase in water diffusivity within the parenchyma. Results showed that mean diffusivity tended to increase systematically between morning and afternoon scans at the interface of grey matter/CSF, and most prominently in the major fissures and the sulci of the brain (55). Another human study aimed to evaluate the influence of circadian rhythms or the effect of sleep by measuring the slow and fast components of the apparent diffusion coefficient (ADC) of water in the brain in 50 healthy participants. Wake versus sleep conditions were compared in 30 subjects, and rested-wakefulness versus wakefulness following one night of sleep-deprivation was compared in 20 subjects. Results of that study indicated that sleep compared to wakefulness was associated with increases in slow-ADC in the cerebellum and left temporal pole and with reductions in fast-ADC in the thalamus, insula, para-hippocampus and striatal regions. In addition, the level of sleep arousal was inversely associated with ADC changes. CSF volume also increased during sleep and was associated with sleep-induced changes in ADC in the cerebellum (56). More recently, a study evaluated high- and low-q space diffusion MRI and DTI acquisitions to determine if interstitial glymphatic flow could be

detected, measured, and mapped using a specially made phantom that combined regions mimicking CSF-filled ventricles and interstitial spaces in the brain. Results of this study demonstrated that all DTI metrics derived from water flowing at a rate of 0.44 ml/min through the bead layer were greatly increased compared to stationary conditions, thus indicating that DTI has the potential to detect dispersive flow within the range of CSF flow rates in human tissues. The dual compartment analysis revealed that the increase in diffusivity measured from evening to morning was driven by an increase in the fractional volume of CSF-like free-water (57).

Diffusion imaging can also be applied to the evaluation of CSF motion within the ventricles or surface subarachnoid space. A study using low b-value diffusion-weighted imaging (DWI) was described for determining characteristic CSF dynamics. In this study, the CSF signal intensity on b = 500 s/mm2 DWI was evaluated in the lateral, 3rd and 4th ventricles, the cerebral sulci and the Sylvian fissure in patients with ventricular dilatation. Findings showed that the CSF signal intensities were significantly reduced in the lateral and 3rd ventricles in patients with ventricular dilatation indicating an alteration in CSF dynamics. In control subjects, the signal void in the Sylvian fissure showed a significant decrease correlating with age, possibly suggesting the occurrence of alterations in CSF dynamics with aging (58).

Clinical implications and future perspectives on the glymphatic system

Visualization of glymphatic system function is thought to have significant benefits for the understanding of the mechanism, prevention and treatment of several disorders of the central nervous system. The first report on the glymphatic system hypothesis by Iliff et al. showed that fluorescently tagged amyloid β was transported by the glymphatic system, and deletion of the aquapoline 4 gene suppressed the clearance of soluble amyloid β. These findings suggested that the glymphatic pathway may remove amyloid β, a peptide thought to be pathogenic in Alzheimer's disease, from the central nervous system (1). An animal experiment showed that glymphatic transport is suppressed in mouse models of Alzheimer's disease and that glymphatic transport is suppressed prior to significant accumulation of amyloid β (59). Moreover, in humans, PET and 18F-florbetaben have been used to measure brain Aβ burden in healthy volunteers tested after a night of rested sleep and after a night of sleep deprivation. This study showed that one night of sleep deprivation, relative to baseline, resulted in a significant increase in Aβ burden in the right hippocampus and thalamus, suggesting that interruption of glymphatic clearance by sleep deprivation may increase ABB in the brain (60). In addition, a study using the a fore mentioned diffusion tensor method suggested that lower diffusivity along the perivascular space

in severe Alzheimer's disease may reflect impairment of the glymphatic system (49).

As mentioned previously, iNPH is also thought to be related to impaired glymphatic function. Intrathecal GBCA injection studies showed decreased GBCA clearance from the subarachnoid space, and suggested reduced glymphatic clearance in iNPH patients (15,20). Metabolic disorder has also been reported to show impairment of the glymphatic system, and an animal study demonstrated that the clearance of cerebrospinal fluid GBCA from the interstitial space was slowed by a factor of three in the hippocampus of Type-2 diabetes mellitus rats compared to non-DM rats (61). Alcoholism is also reportedly linked to glymphatic dysfunction. A two-photon laser scanning microscopy study with fluorescent tracer showed that acute moderate alcohol administration substantially retarded and reduced the entry of CSF into the cerebral parenchyma, thus impairing amyloid β clearance (62). Similarly, in psychiatric disorders, involvement of abnormal CSF dynamics or glymphatic function have been suggested. A prospective study was undertaken to evaluate brain growth trajectories from infancy in children who develop autism spectrum disorder. The presence of excessive extra-axial fluid detected as early as 6 months with a lack of resolution by 24 months is a brain anomaly of infants who later develop autism spectrum disorder (63,64).

Several vascular disorders have been reported to induce dysfunction of the glymphatic system. An animal study to investigate the impact of different stroke subtypes on the glymphatic system using GBCA and MRI was reported in 2014. In that study, the integrity of the glymphatic system was evaluated in 4 different stroke models in mice including subarachnoid hemorrhage, intracerebral hemorrhage, carotid ligature, and embolic ischemic stroke. They showed that subarachnoid hemorrhage and acute ischemic stroke significantly impair glymphatic system perfusion (8). Another study sought to show glymphatic system impairment after subarachnoid hemorrhage. Two-photon laser scanning microscopy with a fluorescent tracer showed that blood components rapidly enter the perivascular space after subarachnoid hemorrhage and penetrate into the perivascular parenchyma throughout the brain, causing events such as cerebral vasospasm, delayed cerebral ischemia, microcirculation dysfunction and widespread perivascular neuroinflammation (65).

As demonstrated above, there are a variety of disorders in which involvement of the glymphatic system have been suggested by animal experiments or human studies. When non-invasive or less-invasive methods for evaluating glymphatic function in human subjects are established, our understanding of the mechanisms behind those disorders will deepen, and the information on glymphatic function may subsequently contribute to the development of treatment strategies for these diseases. For example, the biomarker amyloid β is thought to show the first

abnormalities in Alzheimer's disease, followed by neurodegenerative biomarkers and cognitive symptoms, with neurodegenerative biomarkers showing later abnormalities (66). However, as previously discussed, the impairment of glymphatic function is thought to be one of the causes of amyloid β accumulation which precedes the increase in the amyloid β biomarker. Thus, the evaluation of glymphatic function would represent an earlier biomarker for Alzheimer's disease. Information on glymphatic function may also be helpful for monitoring drug delivery in the central nervous system. We previously proposed a hypothesis for the behavior of Gd after intravenous injection (32), which suggests that glymphatic pathways may exist which bypass the blood brain barrier. The evaluation of glymphatic function would substantially help the development of new methods for delivering a variety of molecules to the brain.

Conclusion

At present, the glymphatic system hypothesis has yet to be firmly established, and several reports have pointed out problems with the hypothesis (67-69). The criticisms of the glymphatic system hypothesis include that the flow resistance of the AQP4 channel is too large to enable bulk flow within the interstitial space (67), that the arterial pulse in the tissue is too small to act as a driving force for bulk flow which would make bulk flow within the tissue impossible (68), and that there are other means by which to drain waste via the arterial wall that forms the intramural peri-arterial drainage (IPAD) pathway (69). However, one key point that no one has criticized is that the CSF and ISF have great importance in brain function and homeostasis. In that sense, the research aimed at visualizing the function and/or dynamics of "neurofluids", that includes all fluid compartments within the CNS, using various methods including MRI techniques will provide significant understanding as to how healthy brain function is maintained in humans.

References

1. Iliff JJ, Wang M, Liao Y, et al. A paravascular pathway facilitates CSF flow through the brain parenchyma and the clearance of interstitial solutes, including amyloid beta. Sci Transl Med 2012;4(147):147ra111.
2. Nedergaard M, Goldman SA. Brain Drain. Sci Am 2016;314(3):44-49.
3. Boespflug EL, Iliff JJ. The Emerging Relationship Between Interstitial Fluid-Cerebrospinal Fluid Exchange, Amyloid-beta, and Sleep. Biol Psychiatry 2018;83(4):328-336.
4. IAEA. "Tracer studies" from web page of International Atomic Energy Agency.
5. Mardor Y, Rahav O, Zauberman Y, et al. Convection-enhanced drug delivery: increased efficacy and magnetic resonance image monitoring. Cancer Res 2005;65(15):6858-6863.
6. Xie L, Kang H, Xu Q, et al. Sleep drives metabolite clearance from the adult brain. Science 2013;342(6156):373-377.
7. Iliff JJ, Lee H, Yu M, et al. Brain-wide pathway for waste clearance captured by contrast-enhanced MRI. J Clin Invest 2013;123(3):1299-1309.
8. Gaberel T, Gakuba C, Goulay R, et al. Impaired glymphatic perfusion after strokes revealed by contrast-enhanced MRI: a new target for fibrinolysis? Stroke 2014;45(10):3092-3096.
9. Siebner HR, Grafin von Einsiedel H, Conrad B. Magnetic resonance ventriculography with gadolinium DTPA: report of two cases. Neuroradiology 1997;39(6):418-422; discussion 422.
10. Speck U. Gadolinium DTPA for intrathecal use. Neuroradiology 1997;39(6):422.
11. Samardzic D, Thamburaj K. Magnetic resonance characteristics and susceptibility weighted imaging of the brain in gadolinium encephalopathy. J Neuroimaging 2015;25(1):136-139.
12. Arlt S, Cepek L, Rustenbeck HH, Prange H, Reimers CD. Gadolinium encephalopathy due to accidental intrathecal administration of gadopentetate dimeglumine. J Neurol 2007;254(6):810-812.
13. Reeves C, Galang E, Padalia R, Tran N, Padalia D. Intrathecal Injection of Gadobutrol: A Tale of Caution. J Pain Palliat Care Pharmacother 2017;31(2):139-143.
14. Provenzano DA, Pellis Z, DeRiggi L. Fatal gadolinium-induced encephalopathy following accidental intrathecal administration: a case report and a comprehensive evidence-based review. Reg Anesth Pain Med 2019.
15. Eide PK. MRI with intrathecal MRI gadolinium contrast medium administration: a possible method to assess glymphatic function in human brain. Acta Radiologica

Open 2015;4(11):1-5.

16. Oner AY, Barutcu B, Aykol S, Tali ET. Intrathecal Contrast-Enhanced Magnetic Resonance Imaging-Related Brain Signal Changes: Residual Gadolinium Deposition? Invest Radiol 2017;52(4):195-197.
17. Algin O, Turkbey B. Intrathecal gadolinium-enhanced MR cisternography: a comprehensive review. AJNR Am J Neuroradiol 2013;34(1):14-22.
18. DelGaudio JM, Baugnon KL, Wise SK, Patel ZM, Aiken AH, Hudgins PA. Magnetic resonance cisternogram with intrathecal gadolinium with delayed imaging for difficult to diagnose cerebrospinal fluid leaks of anterior skull base. Int Forum Allergy Rhinol 2015;5(4):333-338.
19. Nacar Dogan S, Kizilkilic O, Kocak B, Isler C, Islak C, Kocer N. Intrathecal gadolinium-enhanced MR cisternography in patients with otorhinorrhea: 10-year experience of a tertiary referral center. Neuroradiology 2018;60(5):471-477.
20. Ringstad G, Vatnehol SAS, Eide PK. Glymphatic MRI in idiopathic normal pressure hydrocephalus. Brain 2017;140(10):2691-2705.
21. Taoka T, Jost G, Frenzel T, Naganawa S, Pietsch H. Impact of the Glymphatic System on the Kinetic and Distribution of Gadodiamide in the Rat Brain: Observations by Dynamic MRI and Effect of Circadian Rhythm on Tissue Gadolinium Concentrations. Invest Radiol 2018;53(9):529-534.
22. van de Haar HJ, Burgmans S, Jansen JF, et al. Blood-Brain Barrier Leakage in Patients with Early Alzheimer Disease. Radiology 2016;281(2):527-535.
23. Naganawa S, Nakane T, Kawai H, Taoka T. Gd-based Contrast Enhancement of the Perivascular Spaces in the Basal Ganglia. Magnetic Resonance in Medical Sciences 2017;16(1):61-65.
24. Naganawa S, Nakane T, Kawai H, Taoka T. Lack of Contrast Enhancement in a Giant Perivascular Space of the Basal Ganglion on Delayed FLAIR Images: Implications for the Glymphatic System. Magn Reson Med Sci 2017;16(2):89-90.
25. Naganawa S, Nakane T, Kawai H, Taoka T. Differences in Signal Intensity and Enhancement on MR Images of the Perivascular Spaces in the Basal Ganglia versus Those in White Matter. Magn Reson Med Sci 2018;17(4):301-307.
26. Naganawa S, Nakane T, Kawai H, Taoka T. Age Dependence of Gadolinium Leakage from the Cortical Veins into the Cerebrospinal Fluid Assessed with Whole Brain 3D-real Inversion Recovery MR Imaging. Magn Reson Med Sci 2019;18(2):163-169.
27. Absinta M, Ha SK, Nair G, et al. Human and nonhuman primate meninges harbor lymphatic vessels that can be visualized noninvasively by MRI. Elife 2017;6.
28. Louveau A, Smirnov I, Keyes TJ, et al. Structural and functional features of central

nervous system lymphatic vessels. Nature 2015;523(7560):337-341.

29. Kanda T, Ishii K, Kawaguchi H, Kitajima K, Takenaka D. High signal intensity in the dentate nucleus and globus pallidus on unenhanced T1-weighted MR images: relationship with increasing cumulative dose of a gadolinium-based contrast material. Radiology 2014;270(3):834-841.
30. Kanda T, Oba H, Toyoda K, Kitajima K, Furui S. Brain gadolinium deposition after administration of gadolinium-based contrast agents. Jpn J Radiol 2016;34(1):3-9.
31. Kanda T. The New Restrictions on the Use of Linear Gadolinium-based Contrast Agents in Japan. Magn Reson Med Sci 2019;18(1):1-3.
32. Taoka T, Naganawa S. Gadolinium-based Contrast Media, Cerebrospinal Fluid and the Glymphatic System: Possible Mechanisms for the Deposition of Gadolinium in the Brain. Magn Reson Med Sci 2018;17(2):111-119.
33. Tailor DR, Roy A, Regatte RR, et al. Indirect 17(O)-magnetic resonance imaging of cerebral blood flow in the rat. Magn Reson Med 2003;49(3):479-487.
34. Kudo K, Harada T, Kameda H, et al. Indirect Proton MR Imaging and Kinetic Analysis of (17)O-Labeled Water Tracer in the Brain. Magn Reson Med Sci 2018;17(3):223-230.
35. Igarashi H, Tsujita M, Kwee IL, Nakada T. Water influx into cerebrospinal fluid is primarily controlled by aquaporin-4, not by aquaporin-1: 17O JJVCPE MRI study in knockout mice. Neuroreport 2014;25(1):39-43.
36. Connor SE, O'Gorman R, Summers P, et al. SPAMM, cine phase contrast imaging and fast spin-echo T2-weighted imaging in the study of intracranial cerebrospinal fluid (CSF) flow. Clin Radiol 2001;56(9):763-772.
37. Sakas DE, Korfias SI, Wayte SC, et al. Chiari malformation: CSF flow dynamics in the craniocervical junction and syrinx. Acta Neurochir (Wien) 2005;147(12):1223-1233.
38. Yamada S, Miyazaki M, Kanazawa H, et al. Visualization of cerebrospinal fluid movement with spin labeling at MR imaging: preliminary results in normal and pathophysiologic conditions. Radiology 2008;249(2):644-652.
39. Yamada S. Cerebrospinal fluid physiology: visualization of cerebrospinal fluid dynamics using the magnetic resonance imaging Time-Spatial Inversion Pulse method. Croat Med J 2014;55(4):337-346.
40. Ohene Y, Harrison IF, Nahavandi P, et al. Non-invasive MRI of brain clearance pathways using multiple echo time arterial spin labelling: an aquaporin-4 study. Neuroimage 2019;188:515-523.
41. Yamashita S, Isoda H, Hirano M, et al. Visualization of hemodynamics in intracranial

arteries using time-resolved three-dimensional phase-contrast MRI. J Magn Reson Imaging 2007;25(3):473-478.

42. Yatsushiro S, Sunohara S, Hayashi N, et al. Cardiac-driven Pulsatile Motion of Intracranial Cerebrospinal Fluid Visualized Based on a Correlation Mapping Technique. Magn Reson Med Sci 2018;17(2):151-160.
43. Hirayama A, Matsumae M, Yatsushiro S, Abdulla A, Atsumi H, Kuroda K. Visualization of Pulsatile CSF Motion Around Membrane-like Structures with both 4D Velocity Mapping and Time-SLIP Technique. Magn Reson Med Sci 2015;14(4):263-273.
44. Takizawa K, Matsumae M, Hayashi N, et al. The Choroid Plexus of the Lateral Ventricle As the Origin of CSF Pulsation Is Questionable. Neurol Med Chir (Tokyo) 2018;58(1):23-31.
45. Ichikawa S, Motosugi U, Okumura A, Shimizu T, Onishi H. Measurement of Cerebrospinal Fluid Flow Dynamics Using Phase Contrast MR Imaging with Bilateral Jugular Vein Compression: A Feasibility Study in Healthy Volunteers. Magn Reson Med Sci 2018;17(3):265-268.
46. Magdoom KN, Zeinomar A, Lonser RR, Sarntinoranont M, Mareci TH. Phase contrast MRI of creeping flows using stimulated echo. J Magn Reson 2019;299:49-58.
47. Stejskal EO, Tanner JE. Spin Diffusion Measurements: Spin Echoes in the Presence of a Time-Dependent Field Gradient. The Journal of Chemical Physics 1965;42:288-292.
48. Le Bihan D, Breton E, Lallemand D, Grenier P, Cabanis E, Laval-Jeantet M. MR imaging of intravoxel incoherent motions: application to diffusion and perfusion in neurologic disorders. Radiology 1986;161(2):401-407.
49. Taoka T, Masutani Y, Kawai H, et al. Evaluation of glymphatic system activity with the diffusion MR technique: diffusion tensor image analysis along the perivascular space (DTI-ALPS) in Alzheimer's disease cases. Jpn J Radiol 2017;35(4):172-178.
50. Okudera T, Huang YP, Fukusumi A, Nakamura Y, Hatazawa J, Uemura K. Micro-angiographical studies of the medullary venous system of the cerebral hemisphere. Neuropathology 1999;19(1):93-111.
51. Taoka T, Fukusumi A, Miyasaka T, et al. Structure of the Medullary Veins of the Cerebral Hemisphere and Related Disorders. Radiographics 2017;37(1):281-297.
52. Steward C, Venkatraman V, Lui E, et al. Reproducibility of the diffusion of the perivascular space in older adults with dementia. 27th International Society for Magnetic Resonance in Medicine. Montreal; 2019. p. 3425.
53. Cekic M, Yokota H, Ellingson B, Linetsk M, Salamon N. Evaluation of the Glymphatic

System with DTI in Idiopathic Normal Pressure Hydrocephalus. American Society of Neuroradiology Annual Meeting. Vancouver; 2018. p. O-518.

54. Harrison IF, Siow B, Akilo AB, et al. Non-invasive imaging of CSF-mediated brain clearance pathways via assessment of perivascular fluid movement with diffusion tensor MRI. Elife 2018;7.

55. Thomas C, Sadeghi N, Nayak A, et al. Impact of time-of-day on diffusivity measures of brain tissue derived from diffusion tensor imaging. Neuroimage 2018;173:25-34.

56. Demiral SB, Tomasi D, Sarlls J, et al. Apparent diffusion coefficient changes in human brain during sleep - Does it inform on the existence of a glymphatic system? Neuroimage 2019;185:263-273.

57. Komlosh ME, Benjamini D, Williamson NW, Horkay F, Hutchinson EB, Basser PJ. A novel MRI phantom to study interstitial fluid transport in the glymphatic system. Magn Reson Imaging 2019;56:181-186.

58. Taoka T, Naganawa S, Kawai H, Nakane T, Murata K. Can low b value diffusion weighted imaging evaluate the character of cerebrospinal fluid dynamics? Jpn J Radiol 2019;37(2):135-144.

59. Peng W, Achariyar TM, Li B, et al. Suppression of glymphatic fluid transport in a mouse model of Alzheimer's disease. Neurobiol Dis 2016;93:215-225.

60. Shokri-Kojori E, Wang GJ, Wiers CE, et al. beta-Amyloid accumulation in the human brain after one night of sleep deprivation. Proc Natl Acad Sci U S A 2018;115(17):4483-4488.

61. Jiang Q, Zhang L, Ding G, et al. Impairment of the glymphatic system after diabetes. J Cereb Blood Flow Metab 2017;37(4):1326-1337.

62. Liu Q, Yan L, Huang M, et al. Experimental alcoholism primes structural and functional impairment of the glymphatic pathway. Brain Behav Immun 2019.

63. Shen MD, Nordahl CW, Young GS, et al. Early brain enlargement and elevated extra-axial fluid in infants who develop autism spectrum disorder. Brain 2013;136(Pt 9):2825-2835.

64. Shen MD. Cerebrospinal fluid and the early brain development of autism. J Neurodev Disord 2018;10(1):39.

65. Luo C, Yao X, Li J, et al. Paravascular pathways contribute to vasculitis and neuroinflammation after subarachnoid hemorrhage independently of glymphatic control. Cell Death Dis 2016;7:e2160.

66. Jack CR, Jr., Knopman DS, Jagust WJ, et al. Hypothetical model of dynamic biomarkers of the Alzheimer's pathological cascade. Lancet Neurol 2010;9(1):119-128.

67. Jin BJ, Smith AJ, Verkman AS. Spatial model of convective solute transport in brain

extracellular space does not support a "glymphatic" mechanism. J Gen Physiol 2016;148(6):489-501.

68. Asgari M, de Zelicourt D, Kurtcuoglu V. Glymphatic solute transport does not require bulk flow. Sci Rep 2016;6:38635.

69. Albargothy NJ, Johnston DA, MacGregor-Sharp M, et al. Convective influx/glymphatic system: tracers injected into the CSF enter and leave the brain along separate periarterial basement membrane pathways. Acta Neuropathol 2018;136(1):139-152.

Figure legends

Figure 1: Outline of the glymphatic system and concept of "common space" in the brain.
Figure 1a illustrates that perivascular clearance comprises perivascular drainage and the glymphatic pathways. Cerebrospinal fluid (CSF) flows into the brain parenchyma via the periarterial space and enters the interstitial space of the brain tissue via AQP4-controlled water channels, which are localized to the end feet of astrocytes which form the outer wall of the perivascular space. CSF entering the interstitial space removes waste proteins from the tissue, then flows into the perivenous space and is discharged outside the brain.
Figure 1b illustrates the concept of "common space" within the brain. The interstitial and CSF spaces of the brain are regarded as common space, which act not only as supportive structures but also function as spaces for mass transport, immune function, or intercellular signal transmission. The common space is filled with "neurofluids", a term referring to all types of fluids which comprise the CNS, including CSF, ISF, and blood, and fluid exchange occurs among these "neurofluid" compartments.

Figure 2: CSF and brain parenchymal contrast enhancement at multiple time points after *intrathecal* GBCA administration
Reconstructed T1-weighted images in sagittal (top row), axial (middle row) and coronal (bottom row) planes from MRI at baseline (before contrast agent administration) and at four subsequent imaging time points demonstrating time-dependent contrast enhancement of the subarachnoid and intraventricular spaces in an iNPH patient (a) and a reference subject (b). Reflux of gadobutrol into the lateral ventricles is a typical feature of iNPH. In the reference subject, retrodural contrast enhancement can be seen in the sagittal images (top row) at the 1 h, 3 h and 4.5 h time points and is indicative of CSF leakage.
Used from reference (20) : Public Domain Material.

Figure 3: GBCA leakage from the cortical veins into the cerebrospinal fluid after *intravenous* administration
Images from a 49-year-old woman with suspicion of endolymphatic hydrops (a). These images were obtained 4 h after intravenous administration of a single dose of gadolinium-based contrast

agent. The CSF around the cortical veins shows a high signal intensity on three-dimensional real inversion recovery (3D-real IR) images (arrows). Images from a 17-year-old woman with a suspicion of endolymphatic hydrops (b). Enhancement in the CSF around the cortical veins was not observed in this young patient.
Used from reference (26) : Public Domain Material.

Figure 4: Distribution of GBCA in the perivascular space after *intravenous* injection
Magnetic resonance cisternography (MRC) from a 71-year-old woman with suspected endolymphatic hydrops. There is much perivascular space (PVS) in the bilateral basal ganglia (a, arrows). In the pre-contrast heavily T2-weighted FLAIR (hT2-FL) images (b), the PVS has a low-signal intensity. In post-contrast hT2-FL images (c), the PVS has an increased signal intensity (arrows). The CSF also shows an increased signal. Note that some regions of the PVS have a higher signal than the CSF.
Used from reference (23) : Public Domain Material.

Figure 5: Hypothesized mechanism of gadolinium deposition via the glymphatic system
Schematic illustrating our hypothesis for gadolinium deposition. Compared with GBCA in systemic circulation, GBCA that is distributed into the CSF cavity via the glymphatic system can remain in brain tissue for an extended period of time. The authors of this review speculate that the glymphatic system may contribute to the tissue deposition of gadolinium.
Used from reference (32) : Public Domain Material.

Figure 6: Dynamic curves of relative signals after injection of ^{17}O-labeled water
Dynamic curves of relative signal intensity. A bolus injection of saline or ^{17}O was initiated 120 s after starting a scan. Significant drops in signal were observed in the cerebral cortex (a), choroid plexus (d), ventricle (e), and subarachnoid space (f) in the ^{17}O condition, while only slight reductions in signal were noted in the basal ganglia/thalamus (b) and white matter (c). In the cerebral cortex, choroid plexus, and subarachnoid space, the curves are characterized by two phases: an initial signal drop and a plateau phase. In the ventricle, the signals gradually and continuously decreased during the acquisition window.
Used from reference (34) : Public Domain Material.

Figure 7: Concept behind the method of diffusion tensor image analysis along the perivascular space (DTI-ALPS) and outcomes in cases of Alzheimer's disease

(a) Roentgenogram of an injected coronal brain slice showing parenchymal vessels that run horizontally within the slice (white box) at the level of the lateral ventricle body. Reproduced with permission from reference (50). (b) Axial SWI within the slice at the level of the lateral ventricle body indicates that parenchymal vessels run laterally (x-axis). (c) Superimposed color display of DTI onto the SWI (b) showing the distribution of projection fibers (z-axis, blue), association fibers (y-axis, green), and subcortical fibers (x-axis, red). Three ROIs were placed in the area with the projection fibers (projection area), association fibers (association area) and subcortical fibers (subcortical area) to measure diffusivities in the three directions (x, y, z). (d) Schematic indicating the relationship between the orientation of the perivascular space (gray cylinders) and the directions of the fibers. Note that the orientation of the perivascular space is perpendicular to both the projection and association fibers. (e-g) Correlation between directional diffusivity and MMSE scores for the three directions of the three areas (projection, e; association, f; subcortical, g). Diffusivity of the x-axis is plotted in red, y-axis in green, and z-axis in blue. Regression lines are also shown in the same colors with the plots, accompanied by values for the correlation coefficient. Statistically significant correlations are shown as asterisks. In the projection area (e), we found a significant positive correlation between the diffusivity along the perivascular space (x-axis) and MMSE scores. In the association area (f), we found a significant positive correlation between the diffusivity along the perivascular space (x-axis) and MMSE scores. Conversely, there was a significant negative correlation between the diffusivity along the projection fibers (z-axis) in the projection area and MMSE scores. There was also a significant negative correlation between the association fibers (y-axis) in the association area and MMSE scores. These negative correlations may be explained by white matter degeneration in the projection or association fibers due to AD or MCI. (h) Correlation between the ALPS-index and MMSE. Correlations between MMSE and the ALPS-index determined by the following ratio are shown:

ALPS-index = mean (Dxproj, Dxassoc)/mean (Dyproj, Dzassoc).

There was a significant positive correlation ($r = 0.46$, $p = 0.0084$) between the ALPS-index and MMSE scores.

Used from reference (49) with permission.

Figure 1

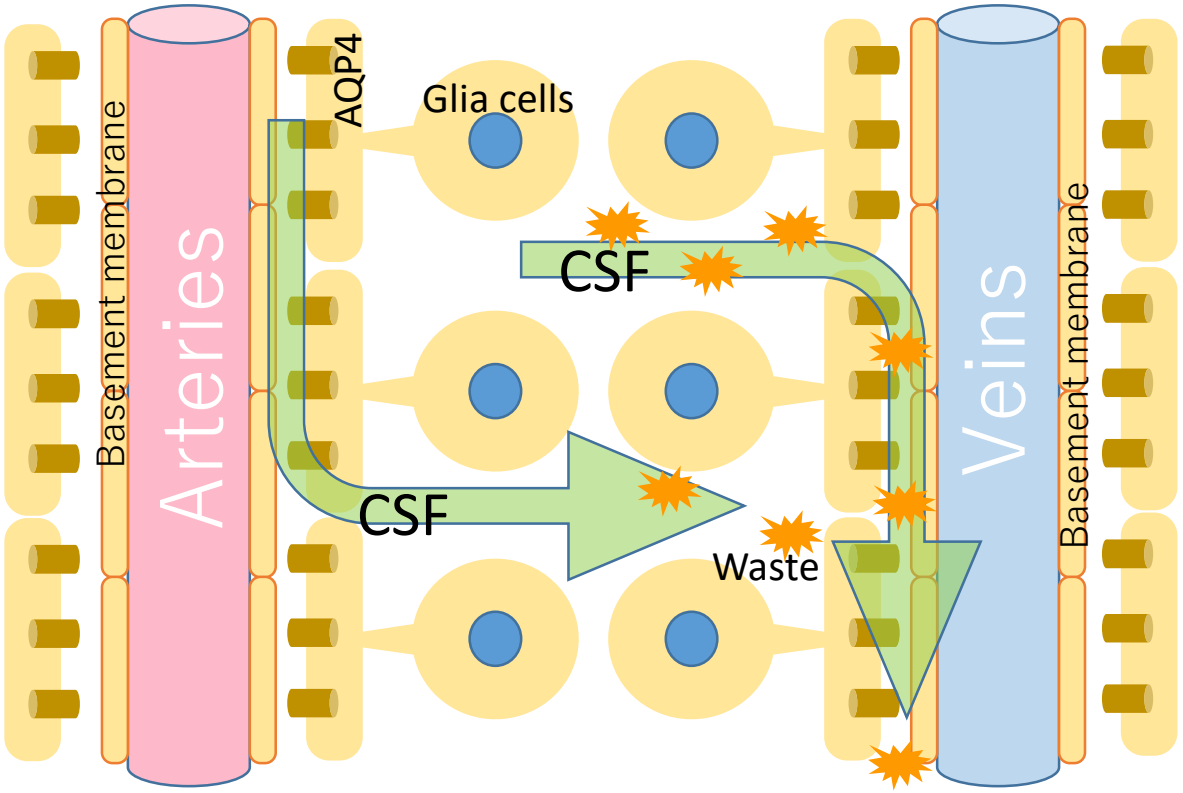
Basement membrane
Arteries
AQP4
Glia cells
CSF
CSF
Waste
Veins
Basement membrane

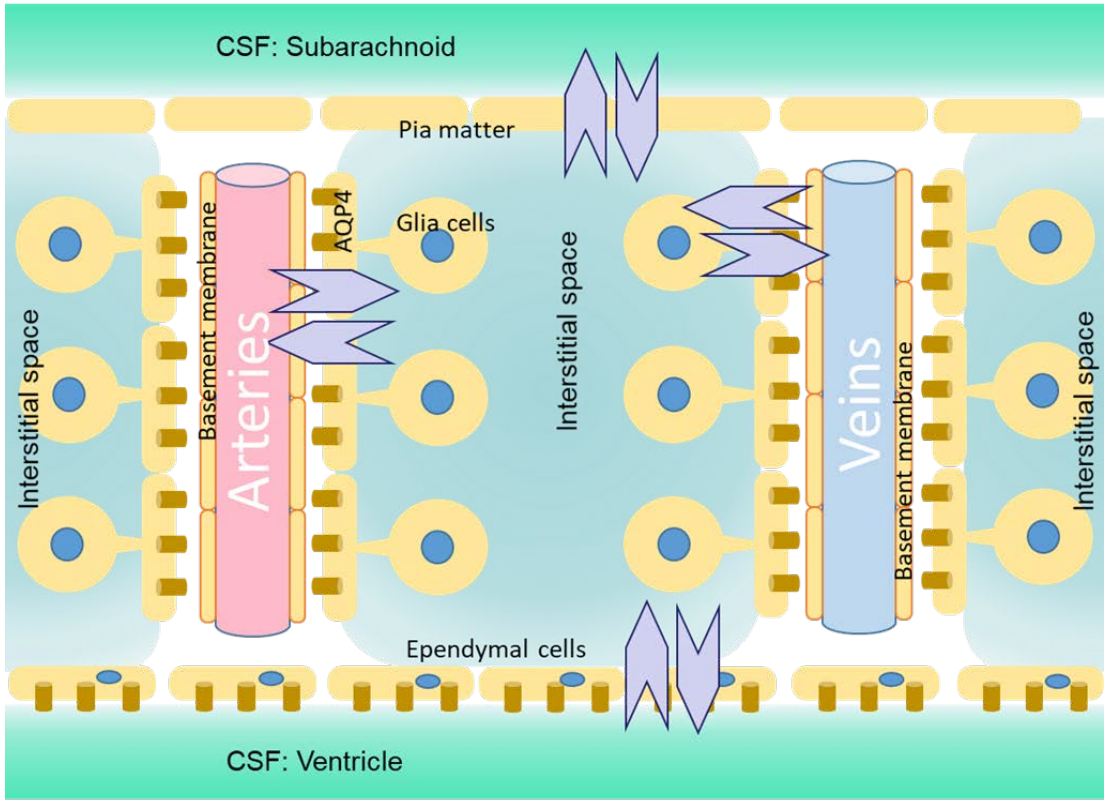
CSF: Subarachnoid
Pia matter
Glia cells
AQP4
Basement membrane
Arteries
Interstitial space
Interstitial space
Veins
Basement membrane
Interstitial space
Ependymal cells
CSF: Ventricle

Figure 2

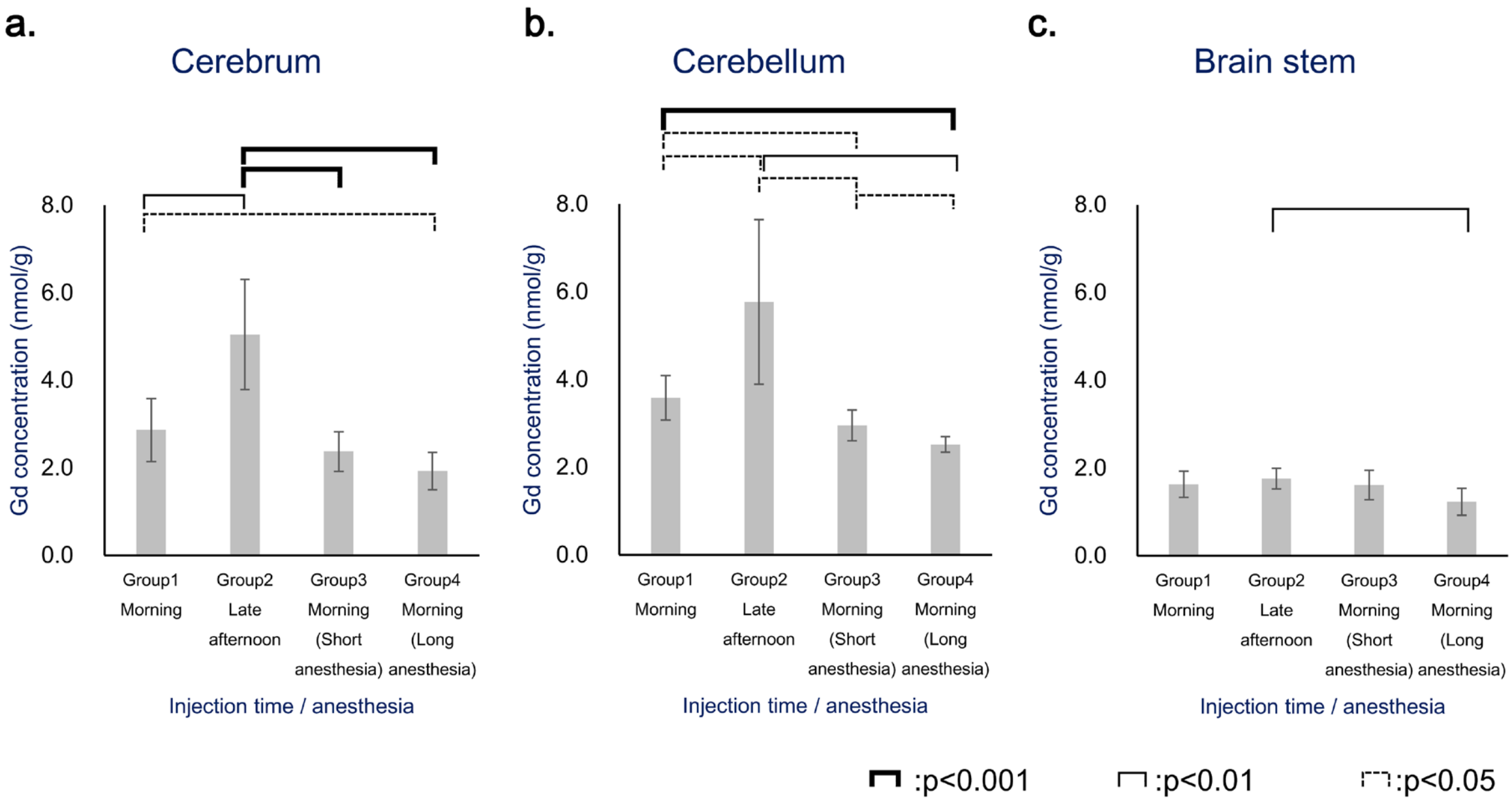
a.
Cerebrum
b.
Cerebellum
c.
Brain stem
Gd concentration (nmol/g)
8.0
6.0
4.0
2.0
0.0
Group1 Morning
Group2 Late afternoon
Group3 Morning (Short anesthesia)
Group4 Morning (Long anesthesia)
Injection time / anesthesia
:p<0.001
:p<0.01
:p<0.05

Figure 3

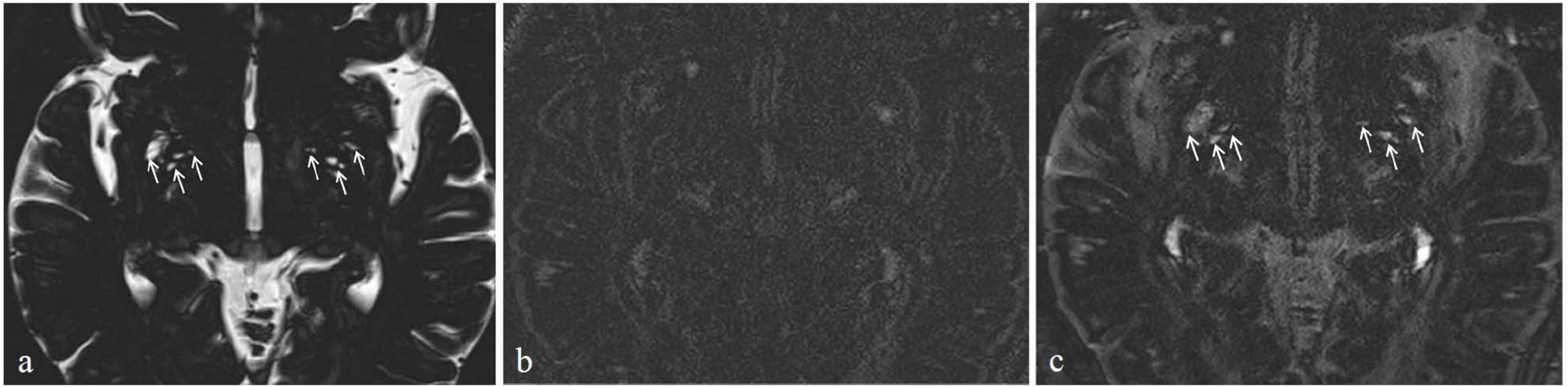

Figure 4

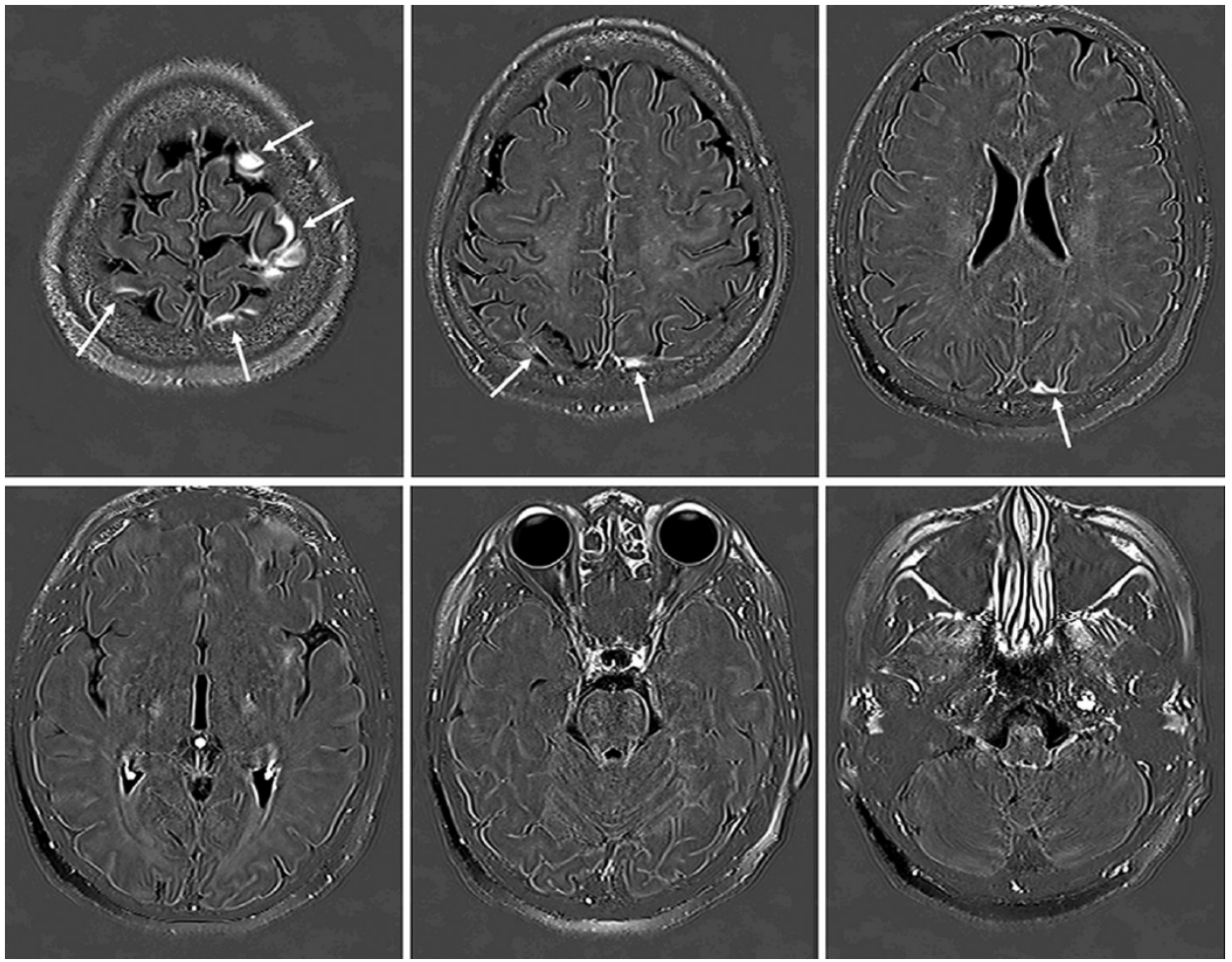

a

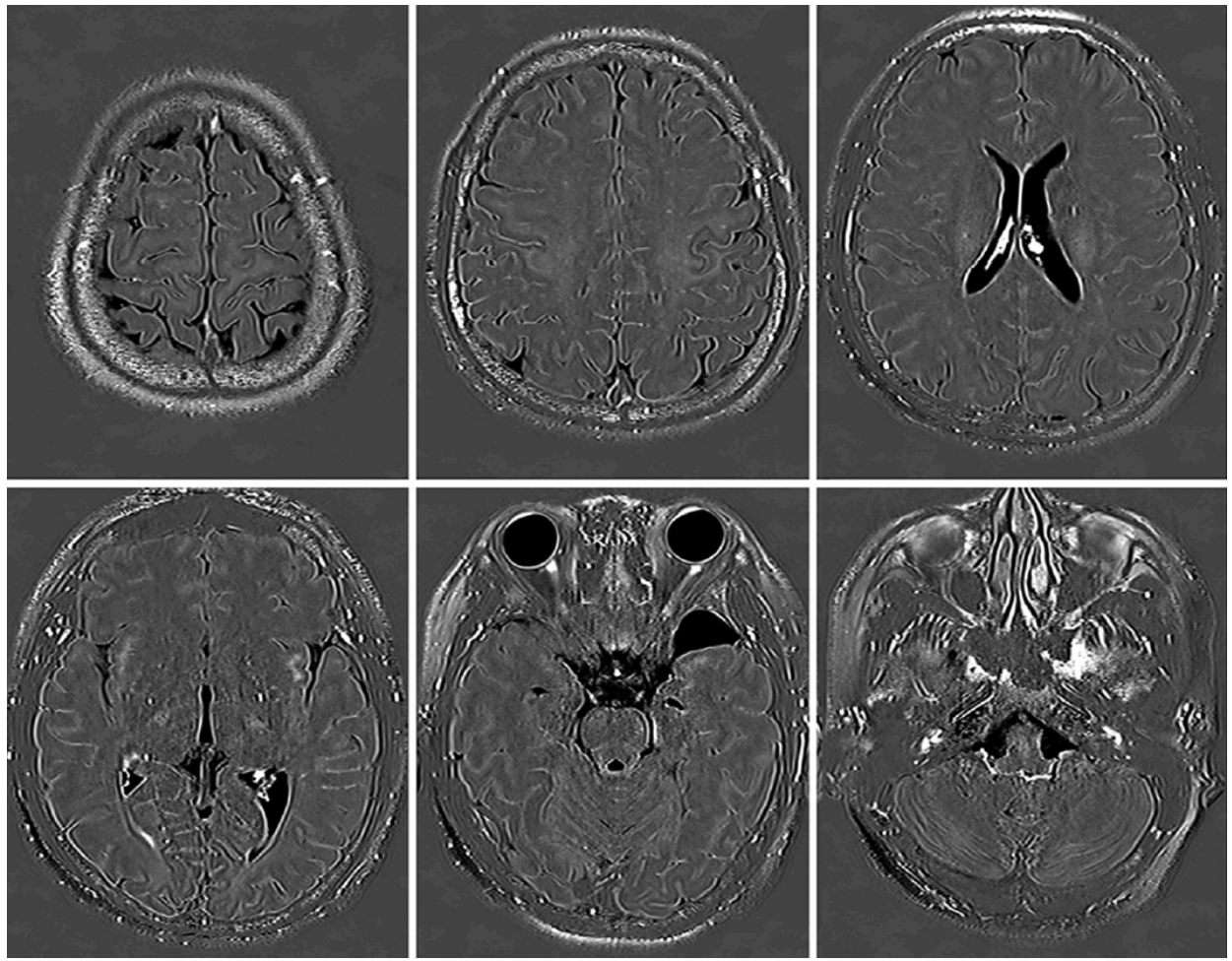

b

Figure 5

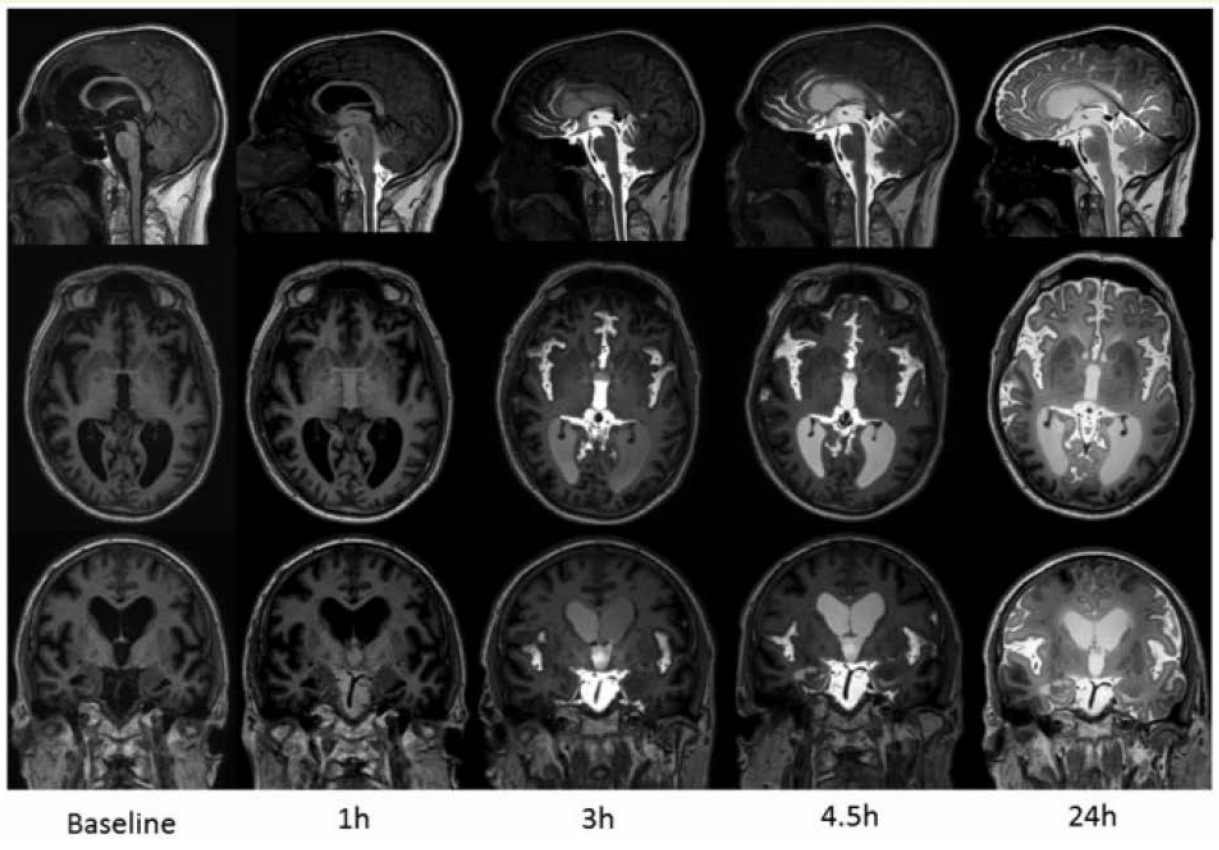

a

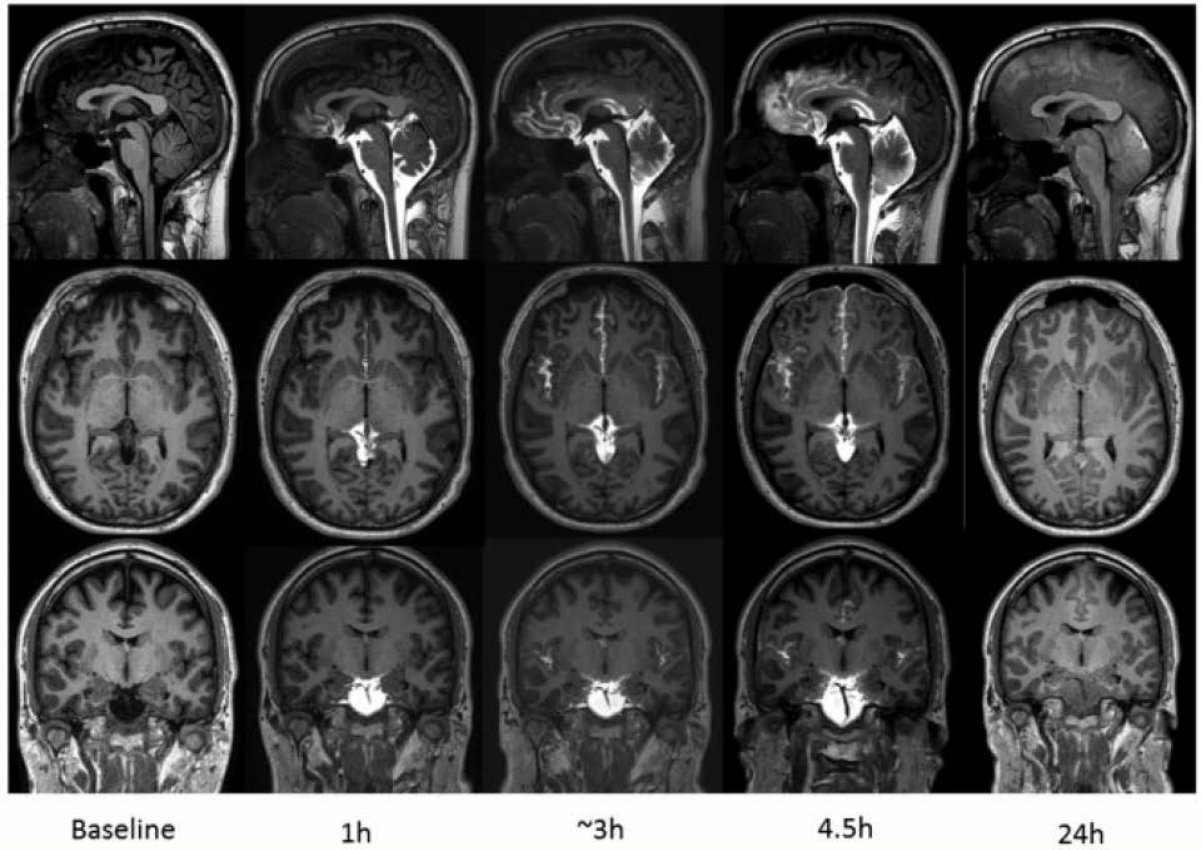

b

Figure 6

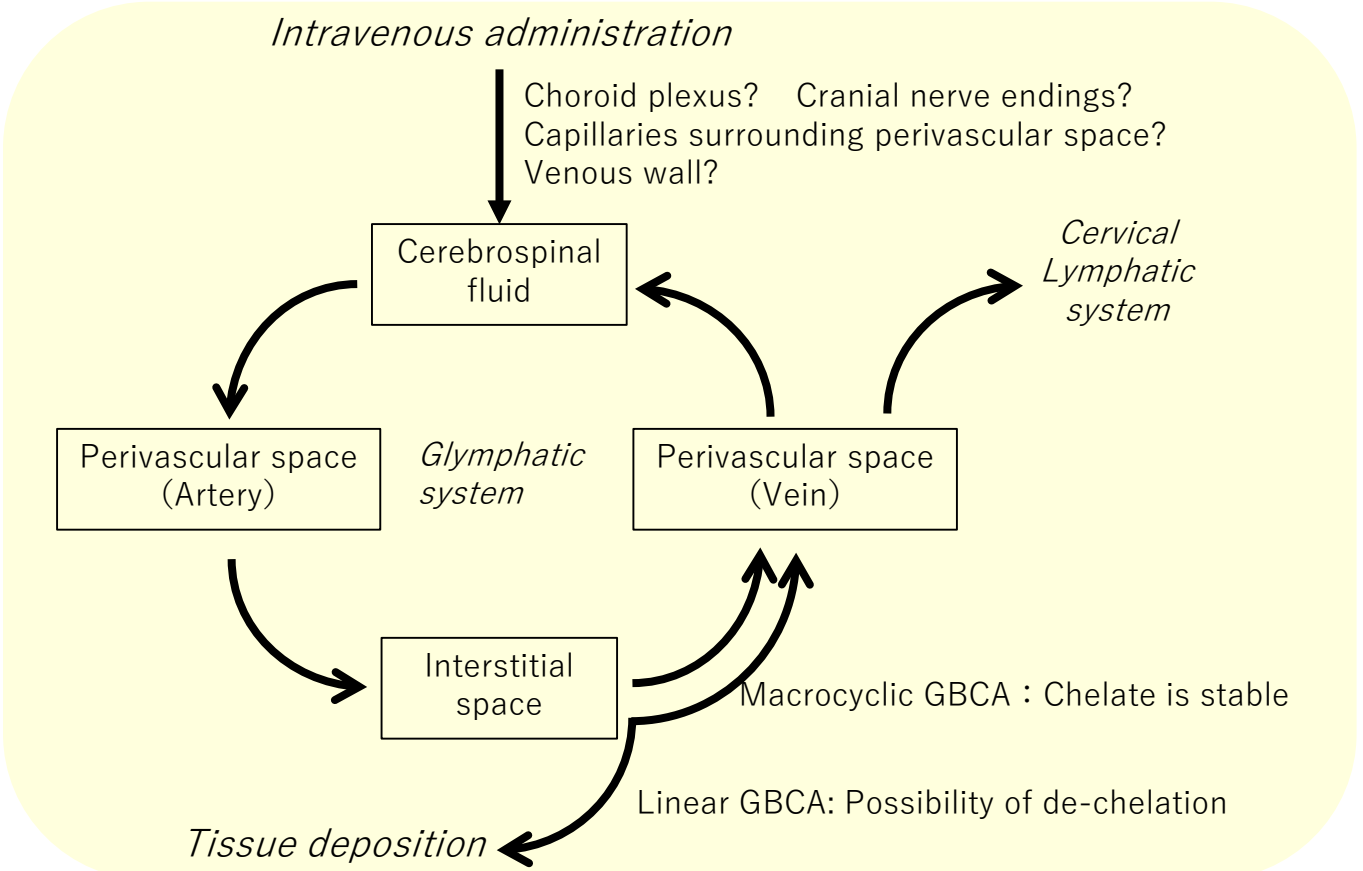
Intravenous administration
Choroid plexus? Cranial nerve endings?
Capillaries surrounding perivascular space?
Venous wall?
Cerebrospinal fluid
Cervical Lymphatic system
Perivascular space (Artery)
Glymphatic system
Perivascular space (Vein)
Interstitial space
Macrocyclic GBCA：Chelate is stable
Linear GBCA: Possibility of de-chelation
Tissue deposition

Figure 7

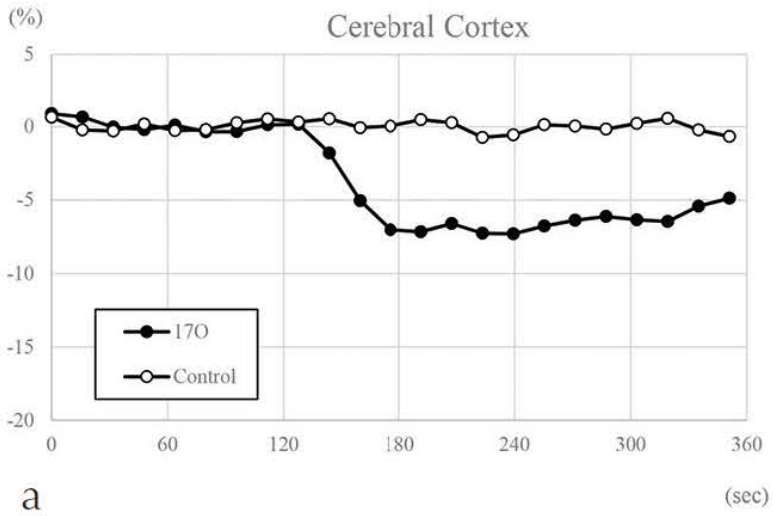

a

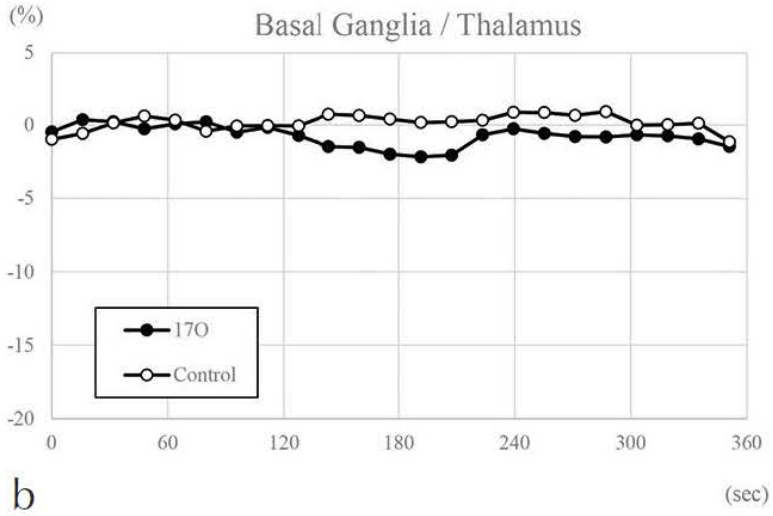

b

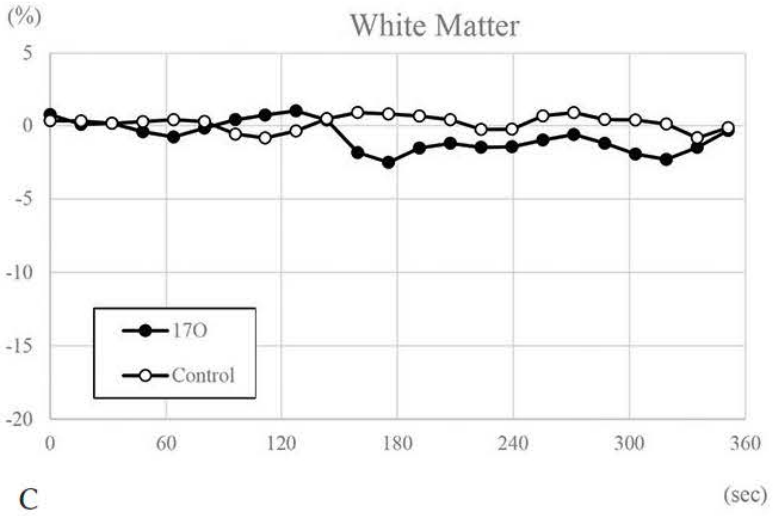

c

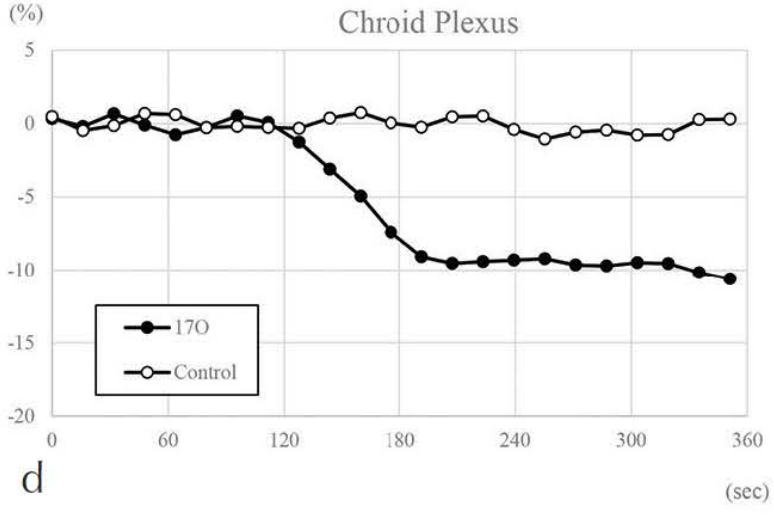

d

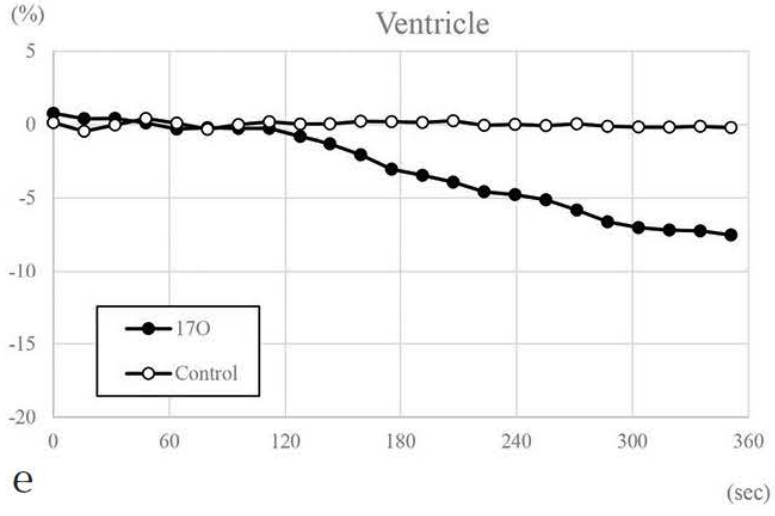

e

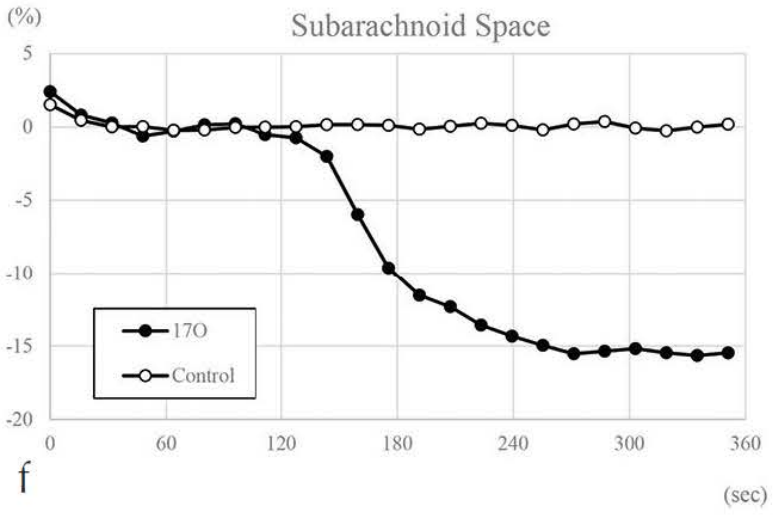

f

Figure 8

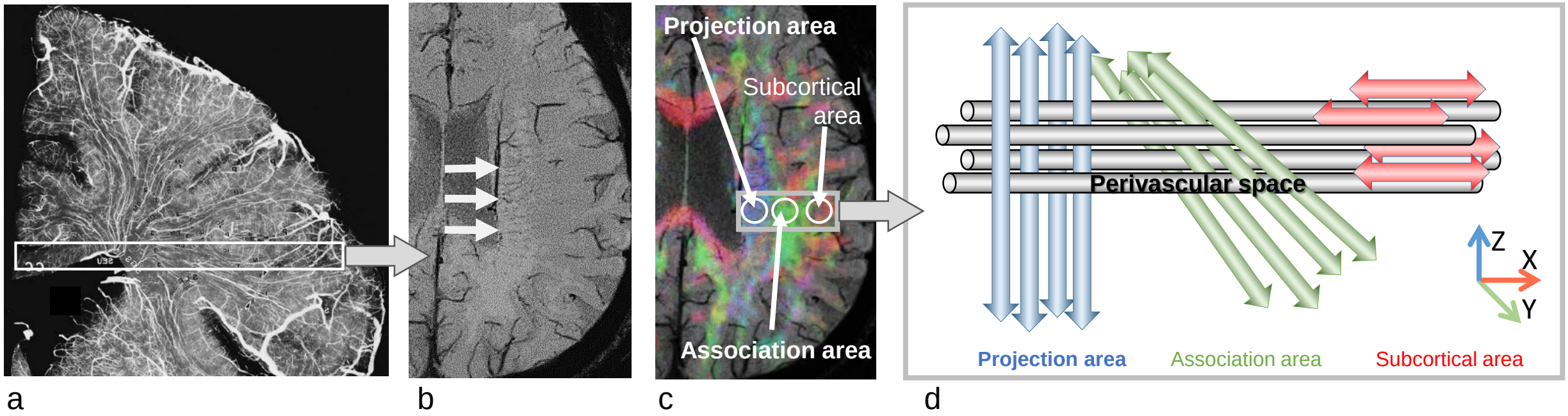
Projection area
Subcortical area
Association area
Perivascular space
Z
X
Y
Projection area
Association area
Subcortical area
a
b
c
d

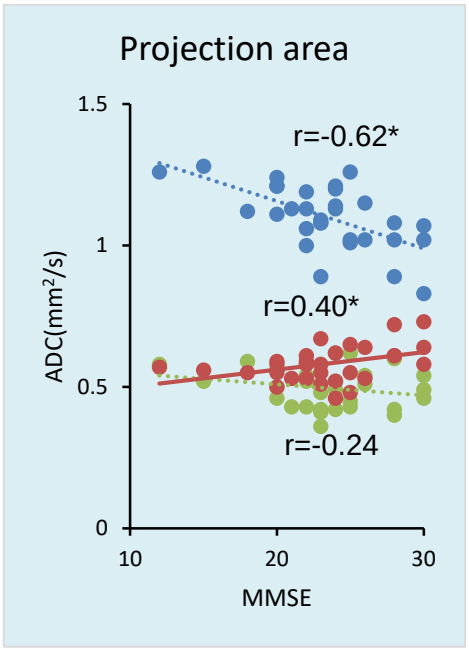
Projection area
r=-0.62*
r=0.40*
r=-0.24
ADC(mm²/s)
MMSE
e

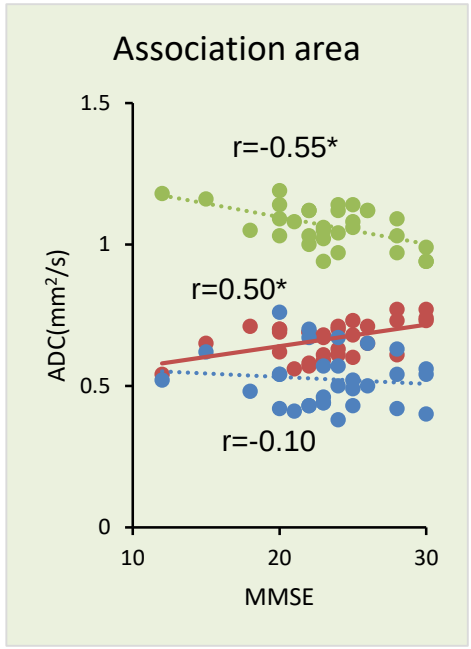
Association area
r=-0.55*
r=0.50*
r=-0.10
ADC(mm²/s)
MMSE
f

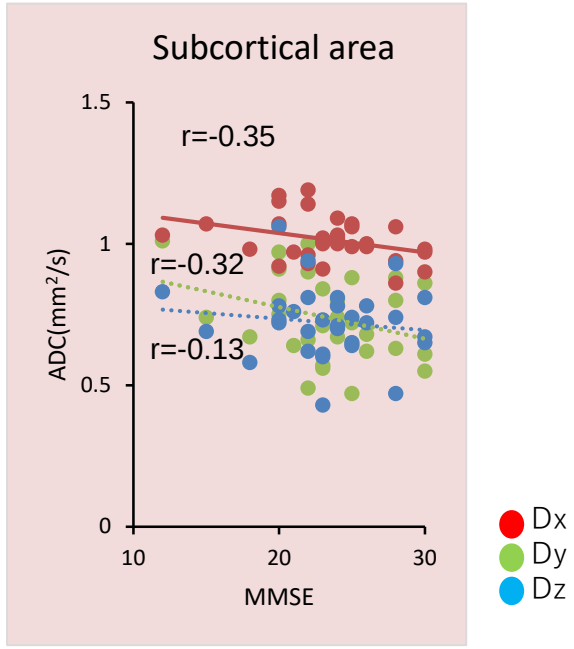
Subcortical area
r=-0.35
r=-0.32
r=-0.13
ADC(mm²/s)
MMSE
Dx
Dy
Dz
g

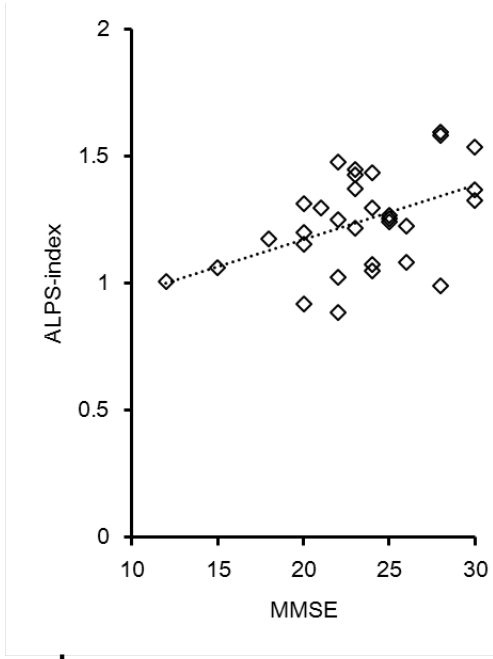
ALPS-index
MMSE
h